⌘ *Author's Choice*

THE JOURNAL OF BIOLOGICAL CHEMISTRY VOL. 287, NO. 25, pp. 21110–21120, June 15, 2012

Inhibition of Autophagy Rescues Palmitic Acid-induced Necroptosis of Endothelial Cells*[S]

Received for publication, October 31, 2011, and in revised form, April 3, 2012 Published, JBC Papers in Press, May 3, 2012, DOI 10.1074/jbc.M111.319129

Muhammad Jadoon Khan[‡1], Muhammad Rizwan Alam[‡1], Markus Waldeck-Weiermair[‡], Felix Karsten[‡], Lukas Groschner[‡], Monika Riederer[‡], Seth Hallström[§], Patrick Rockenfeller[¶], Viktoria Konya[‖], Akos Heinemann[‖], Frank Madeo[¶], Wolfgang F. Graier[‡], and Roland Malli[‡2]

From the [‡]Institute of Molecular Biology and Biochemistry, Center of Molecular Medicine, the [§]Institute of Physiological Chemistry, Center of Physiological Medicine, and the [‖]Institute of Experimental and Clinical Pharmacology, Center of Molecular Medicine, Medical University of Graz, 8010 Graz, Austria and the [¶]Center for Molecular Biosciences, University of Graz, 8010 Graz, Austria

Background: Accumulation of palmitic acid in endothelial cells induces cellular dysfunction and death.
Results: Palmitic acid triggers Ca^{2+}-dependent autophagy, which results in programmed necrotic death (necroptosis) of endothelial cells.
Conclusion: Autophagy promotes lipotoxic signaling of palmitic acid in endothelial cells leading to necroptosis.
Significance: Showing a new molecular mechanism of palmitic acid-induced cytotoxicity may reveal novel strategies in the treatment of diseases related to lipid overload.

Accumulation of palmitic acid (PA) in cells from nonadipose tissues is known to induce lipotoxicity resulting in cellular dysfunction and death. The exact molecular pathways of PA-induced cell death are still mysterious. Here, we show that PA triggers autophagy, which did not counteract but in contrast promoted endothelial cell death. The PA-induced cell death was predominantly necrotic as indicated by annexin V and propidium iodide (PI) staining, absence of caspase activity, low levels of DNA hypoploidy, and an early ATP depletion. In addition PA induced a strong elevation of mRNA levels of ubiquitin carboxyl-terminal hydrolase (CYLD), a known mediator of necroptosis. Moreover, siRNA-mediated knockdown of CYLD significantly antagonized PA-induced necrosis of endothelial cells. In contrast, inhibition and knockdown of receptor interacting protein kinase 1 (RIPK1) had no effect on PA-induced necrosis, indicating the induction of a CYLD-dependent but RIPK1-independent cell death pathway. PA was recognized as a strong and early inducer of autophagy. The inhibition of autophagy by both pharmacological inhibitors and genetic knockdown of the autophagy-specific genes, vacuolar protein sorting 34 (VPS34), and autophagy-related protein 7 (ATG7), could rescue the PA-induced death of endothelial cells. Moreover, the initiation of autophagy and cell death by PA was reduced in endothelial cells loaded with the Ca^{2+} chelator 1,2-*bis*(*o*-aminophenoxy)ethane-*N*,*N*,*N*′,*N*′-tetraacetic acid-(acetoxymethyl) ester (BAPTA-AM), indicating that Ca^{2+} triggers the fatal signaling of PA. In summary, we introduce an unexpected mechanism of lipotoxicity in endothelial cells and provide several novel strategies to counteract the lipotoxic signaling of PA.

Palmitic acid (PA)[3] is the most abundant saturated free fatty acid in the bloodstream and is known to induce cellular dysfunction and cell death in a number of cell types. The lipotoxic effect of PA appears predominantly when cells from nonadipose tissues are chronically exposed to high levels of this saturated fatty acid. This leads to lipid overload, which is particularly relevant in the pathology of obesity and type 2 diabetes (1). Numerous studies using cultured cells such as pancreatic beta cells (2), cardiomyocytes (3), hepatocytes (4), and other cell lines (5), improved our understanding of the potential molecular mechanisms behind PA-induced cytotoxic signaling and cell damage. However, little is known about respective processes in endothelial cells although this cell type is particularly known to suffer from hyperlipidemia leading to vascular dysfunction, a main cause for morbidity and mortality in industrial countries (6). Notably, many studies point to mitochondria as initial targets of the lipotoxic effect of PA or other fatty acids (7), whereupon disturbed synthesis of cardiolipin, a mitochondria-specific phospholipid, and mitochondrial generation of reactive oxygen species is believed to facilitate cell death by apoptosis (1). Interestingly, there are some reports in which a role of PA in the initiation of autophagy (8) and lysosomal dysfunction is emphasized (9). Macroautophagy commonly known as autophagy is an evolutionarily conserved mechanism by which cells sequester and transport damaged organelles and macromolecules for degradation in lysosomes. This process is known to serve as a survival mechanism in states of starvation (10), oxidative stress (11), and other harmful conditions where it helps to replenish the cell with nutrients. The process may sometimes become detrimental by turning into type II programmed cell

* This work was supported in part by Austrian Science Fund (FWF) Grants F3010-B05 (SFB LIPOTOX), P21857-B18, P22553-B18, and P23490.
⌘ *Author's Choice*—Final version full access.
[S] This article contains supplemental Figs. S1–S4 and Movies S1 and S2.
[1] Supported by the FWF within the Molecular Medicine and Neuroscience Ph.D. programs at the Medical University of Graz.
[2] To whom correspondence should be addressed: Harrachgasse 21/III, Graz, Austria. Tel.: 43-316-380-7565; Fax: 43-316-380-9615; E-mail: roland.malli@medunigraz.at.

[3] The abbreviations used are: PA, palmitic acid; $[Ca^{2+}]_{cyto}$, cytosolic Ca^{2+} concentration; 3-MA, 3-methyladenine; ATG7, autophagy-related protein 7; BAPTA/AM, 1,2-*bis*(*o*-aminophenoxy)ethane-*N*,*N*,*N*′,*N*′-tetraacetic acid-tetra(acetoxymethyl)ester; BHQ, 2,5-di-*tert*-butylhydroquinone; LC3, microtuble-associated protein light chain 3; MTT, 3-(4,5-dimethylthiazol-2-yl)-2,5-diphenyltetrazolium bromide; OA, oleic acid; PI, propidium iodide; VPS34, vacuolar protein sorting 34; Z, benzyloxycarbonyl; fmk, fluoromethylketone; RFP, red fluorescent protein; ER, endoplasmic reticulum.

death referred to as autophagic cell death (12, 13), which is thought to be achieved by the same autophagy machinery but with a different outcome (14). Autophagy is known to be associated with organelle dysfunction and cellular damage and may lead to cell death either by extensive self-eating (15), or by the activation of apoptosis (16) or necrosis (14, 17).

This study was designed to investigate a putative role of autophagy in the lipotoxic signaling of PA in endothelial cells. Here, we demonstrate that PA induces programmed necrotic death (necroptosis) of endothelial cells via the initiation of enhanced autophagy. This is an unexpected finding, which points to new possibilities in antagonizing lipotoxicity.

EXPERIMENTAL PROCEDURES

Materials—Cell culture materials were obtained from Invitrogen and fetal calf serum and media supplements were from PAA Laboratories (Pasching, Austria). Palmitic acid, oleic acid, 3-(4,5-dimethylthiazol-2-yl)-2,5-diphenyltetrazolium bromide (MTT), histamine, 2, 5-di-*tert*-butylhydroquinone (BHQ), wortmannin, and 3-methyladenine (3-MA) were purchased from Sigma and Fura-2/AM and BAPTA-AM were obtained from Molecular Probes and Invitrogen. All other chemicals were from Roth (Karlsruhe, Germany), if not mentioned otherwise. Antibody against LC3 was obtained from Cell Signaling (New England Biolabs), and β-actin was from Santa Cruz Biotechnology.

Cell Culture—Endothelial cells from the human umbilical vein endothelial cell-derived cell line EA.hy926 (18) at passages 45 to 85 were used in this study. Cells were grown in DMEM containing 10% FCS, 1% HAT (5 mM hypoxanthin, 20 μM aminopterin, and 0.8 mM thymidine), 50 units/ml of penicillin, 50 μg/ml of streptomycin, and were maintained at 37 °C in 5% CO_2 atmosphere.

Free Fatty Acid Treatment—Cells were treated with the free fatty acids, PA, or oleic acid (OA) complexed to bovine serum albumin (BSA) in a ratio of 6:1 (free fatty acid:BSA) in full culture medium (19). As a control BSA alone was added to cells. Cells were pretreated with the mentioned chemicals 20 min before the addition of free fatty acid or BSA.

Plasmid Construction of Venus-LC3—Venus-LC3 was cloned in the multiple cloning site of pcDNA 3.1 cloning vector (Invitrogen, Austria) using BamHI and EcoRI restriction sites followed by subcloning Venus using restriction sites KpnI and BamHI.

siRNA Design and Validation—siRNA against ATG7 (5′-CAGUGGAUCUAAAUCUCAAACUGAU-3′) was designed as described previously (20), whereas siRNA against VPS34 (5′-GUGUGAUGAUAAGGAAUAU-3) was designed as described by Gao *et al.* (21). CYLD siRNA (5′-CGAAGAGGCTGAATCATAA-3′) was designed as described by Stegmeier *et al.* (22), whereas RIPK1 (CTGGGCGATATTTGCAAATAACC) was designed using the Microsynth siRNA designing tool (Microsynth, Balgach, Switzerland). Knockdown efficiency of individual siRNA was validated by real time quantitative PCR (RT-qPCR) using sequence-specific primers for VPS34 (VPS34-F, 5′-GGGATTAGTGCTGAGGTCATG-3′, and VPS34-R, 5′-AGTCTATGTGGAAGAGTTTGCC-3′), CYLD (CYLD-F, 5′-TGGGATGGAAGATTTGATGGAG-3′ and CYLD-R, 5′-CATAAAGGCAAGTTTGGGAGG-3′), RIPK1 (RIPK1-F, 5′-CATGGAAAAGGCGTGATACAC-3′, and RIPK1-R, 5′-ACTTCCCTCAGCTCATTGTG-3′), and ATG7 (ATG7-F, 5′-TTTTGCTATCCTGCCCTCTG-3′, and ATG7-R, 5′-GCTGTGACTCCTTCTGTTTGAC-3′), *versus* the control siRNA. All siRNAs were obtained from Microsynth.

Transfection of siRNA and Plasmid—Cells were grown on 30-mm glass coverslips to 80% confluence and transfected with either siRNA or plasmid using the TransFast™ transfection reagent from Promega (Madison, WI). 50 pmol of the respective siRNA(s) were mixed with transfection reagent in 0.5 ml of DMEM without FCS and incubated at room temperature for 15 min. The mixture was applied to cells under normal culture conditions and diluted with 0.5 ml of serum-free DMEM after 1 h. Cells were incubated overnight and the medium was exchanged with complete culture medium after 18–20 h. For overexpression of Venus-LC3 cells were transfected with 1 ml of serum-free DMEM containing 2 μg of plasmid DNA and 4 μl of TransFast. The medium was complemented after 1 h with 1 ml of full culture medium. Cells were incubated for 4 h and the medium was replaced by complete culture medium. All experiments were performed 48–72 h after transfection.

MTT Assay—Cellular viability was measured using MTT. For the MTT assay, endothelial cells were plated in a 24-well plate. After each treatment cells were washed with warm PBS and incubated for 3 h with normal cell culture medium containing 0.5 mg/ml of MTT (Sigma). Cells of each well were washed twice with ice-cold PBS and lysed with 200 μl of a lysis buffer composed of 0.04 M HCl in absolute isopropyl alcohol. A 24-well plate was then continuously shaken at room temperature for 15 min on a microplate shaker. The absorbance was subsequently measured at 530 nm on a Wallace PerkinElmer Victor 1420–004 multilabel plate reader. Data were normalized to respective controls and represented as percent viability of the controls.

Annexin V and Propidium Iodide (PI) Staining—Cells were washed with warm PBS prior to the usage of the Annexin V-Fluos® staining kit from Roche Biodiagnostics (Roche Diagnostics GmbH). According to the manufacturers protocol 20 μl of Annexin V-Fluos were diluted in 1 ml of incubation buffer and 20 μl of propidium iodide was added. 100 μl of this mixture were added directly to the cells. After 20 min of incubation cells were analyzed on an array confocal laser scanning microscope described below.

ATP Measurement—Separation of adenine nucleotides was performed on a Hypersil ODS column (5 μm, 250 × 4 mm inner diameter), using a L2200 autosampler, two L-2130 HTA pumps, and a L2450 diode array detector (all from VWR Hitachi). The wavelength for detection of adenine nucleotides was set at 254 nm. EZchrom Elite (VWR) was used for data acquisition and analysis. After trypsinization and mild centrifugation (supernatant discarded) cellular proteins of EA.hy926 cells were precipitated with 250 μl of perchloric acid (0.4 mol/liter). After centrifugation (12,000 × *g*), 100 μl of the supernatant was neutralized with 10–12 μl of potassium carbonate (2 mol/liter, 4 °C). The supernatant obtained after centrifugation was used for HPLC analysis (injection volume: 40 μl). The pellets of the acid extract were dissolved in 0.5 ml of sodium hydroxide (0.1

mol/liter) and used for protein determination (BCA assay, Pierce).

Western Blotting—Endothelial cells were washed twice with ice-cold PBS and total cellular protein was isolated by lysing the cells with RIPA buffer containing a protease inhibitor mixture (Sigma). The protein concentration was measured using a Thermo Scientific Pierce BCA protein assay kit (Thermo Fisher Scientific Inc.). 30 μg of protein were separated by SDS-PAGE and transferred to a nitrocellulose membrane. The membrane was incubated with the primary antibody at 4 °C overnight and the primary antigen-antibody complex was detected by incubating the blot with a horseradish peroxidase-conjugated secondary antibody at room temperature for 1 h. The membrane was further developed with the ECL Plus Western blotting detection system (GE Healthcare). To control the equal amount of protein loading all detected proteins were densitometrically normalized to β-actin.

Cytosolic Ca^{2+} Measurement—For cytosolic Ca^{2+} measurements the Fura-2 technique was used as described previously (23). Cells were loaded with Fura-2/AM and rested prior to experiments in a Hepes-buffered solution containing (in mM): 135 NaCl, 5 KCl, 2 $CaCl_2$, 1 $MgCl_2$, 10 Hepes acid, 2.6 $NaHCO_3$, 0.44 KH_2PO_4, 0.34 Na_2HPO_4, 10 D-glucose, 0.1% vitamins, 0.2% essential amino acids, and 1% penicillin/streptomycin; pH was adjusted to 7.4 with NaOH. For experiments in intact cells Ca^{2+} containing experimental buffer was composed of (in mM): 138 NaCl, 5 KCl, 2 $CaCl_2$, 1 $MgCl_2$, 10 D-glucose, and 10 Hepes acid; pH was adjusted to 7.4 with 1 M NaOH. For experiments in Ca^{2+}-free solution, experimental buffer containing 1 mM EGTA instead of $CaCl_2$ was used.

Experiments were performed on a Nikon inverted microscope (Eclipse 300TE, Nikon, Vienna) equipped with CFI Plan Fluor ×40 oil immersion objective lens (NA 1.3, Nikon, Vienna, Austria), an epifluorescence system (150 W XBO; Optiquip, Highland Mills, NY), a computer-controlled *Z*-stage (Ludl Electronic Products, Haawthrone, NY), and a liquid-cooled charged-coupled device camera (−30 °C; Quantix KAF 1400G2, Roper Scientific, Acton, MA). All devices were controlled by MetaFluor4.0 software (Visitron Systems, Puchheim, Germany). Fura-2/AM was simultaneously excited at 340 nm (340HT15, Omega Optical, Brattleboro, VT) or 380 nm (380HT15, Omega Optical) and emission was monitored at 510 nm (510WB40, Omega Optical). Cytosolic Ca^{2+} was expressed as the ratio of emitted fluorescence at 340 and 380 nm (F_{340}/F_{380}). Cells were perfused using a perfusion system and stimulated in nominal Ca^{2+}-free experimental buffer containing 100 μM histamine and 15 μM BHQ.

RT-qPCR—Total RNA was isolated using RNeasy mini kit from Qiagen. First strand cDNA synthesis was performed with 2 μg of RNA. Real time PCR was performed using the light cycler 480 (Roche Diagnostics) and QuantiFast SYBR Green PCR kit (Qiagen). Gene-specific primers were designed using the real time PCR tool from IDT Scitools (Integrated DNA Technologies) and obtained from Invitrogen. PCRs were performed in 10 μl with the following parameters: 95 °C for 5 min followed by two steps cycling at 95 °C for 10 s and 60 °C for 30 s for 40 cycles.

Array Confocal Laser Scanning Microscopy—High resolution imaging of annexin V/PI and Venus-LC3 was performed using an array confocal laser scanning microscope. The array confocal laser scanning microscope was built on an inverse, fully automatic microscope (Axio Observer.Z1 from Zeiss, Göttingen, Germany) that was equipped with a ×100 objective (Plan-Fluor ×100/1.45 Oil, Zeiss), a Nipkow-based confocal scanner unit (CSU-X1, Yokogawa Electric Cooperation, Tokyo, Japan), a motorized filter wheel (CSUX1FW, Yokogawa Electric Cooperation) on the emission side, and an AOTF-based laser merge module for laser lines 405, 445, 473, 488, 515, and 561 nm (Visitron Systems). Emission was acquired with a charged-coupled device camera (CoolSNAP-HQ, Photometrics, Tucson, AZ). All devices were controlled by VisiView Premier acquisition software (Visitron Systems).

Detection of Caspase-3 Activity Using Casper3-GR—Cells expressing the Förster resonance energy transfer (FRET)-based sensor Casper3-GR (24) (Casper3-GR vector DNA was purchased from BioCat GmbH, Heidelberg, Germany) for caspase-3 activity were imaged on the array confocal laser scanning microscope using a ×40 objective (Zeiss). The following 3 channels for imaging the red fluorescence protein (RFP), the green fluorescence protein (GFP), and the FRET signal between GFP and RFP were used to determine the cleavage of the sensor by caspase-3: RFP channel, excitation 561 nm laser line, emission was collected at 630/75 nm; GFP channel, excitation 488 nm laser line, emission was measured at 525/40 nm; FRET between GFP and RFP, excitation 488 nm laser line, emitted light was imaged at 630/75 nm. The 3 channels were imaged consecutively using the same exposure times (500 ms). Caspase-3 activity was expressed as the ratio of GFP/FRET. 24 h after transfection cells were treated with BSA or PA for 16–18 h. Staurosporin was used as a positive control. For more details see supplemental Fig. 2.

Quantification of DNA Hypoploidy by Flow Cytometry—Endothelial cells were grown to 90% confluence and treated with BSA, 0.5 mM PA, and 300 nM staurosporine for 16 h. Cells were trypsinized followed by washing with PBS, and pelleted by centrifugation. Cells were fixed by incubation with 70% ethanol on ice for 15 min. Cells were pelleted and resuspended in 500 μl of PI solution (in PBS: 50 μg/ml of PI, 0.1 mg/ml of RNase A, 0.05% Triton X-100) and incubated at 37 °C for 40 min. The PI solution was diluted by adding 3 ml of PBS and cells were pelleted by centrifugation. Cells were resuspended in 500 μl of PBS and analyzed by flow cytometry (FACSCalibur, BD Biosciences). Individual cells were distinguished from cell debris and aggregated cells by means of forward-scatter/side-scatter gating, and PI fluorescence intensity was measured in 10,000 cells (25).

Statistical Analysis—Data shown represent the mean ± S.E. Statistical analyses were performed with unpaired Student's *t* test. *n* represents the number of independent experiments and $p < 0.05$ was considered to be significant.

RESULTS

PA Induces Necrotic Cell Death in Endothelial Cells—First we tested the susceptibility of the endothelial cell line, EA.hy926, to PA-induced cell death. For this purpose cells were treated with a complex of PA and BSA and cell viability was measured with

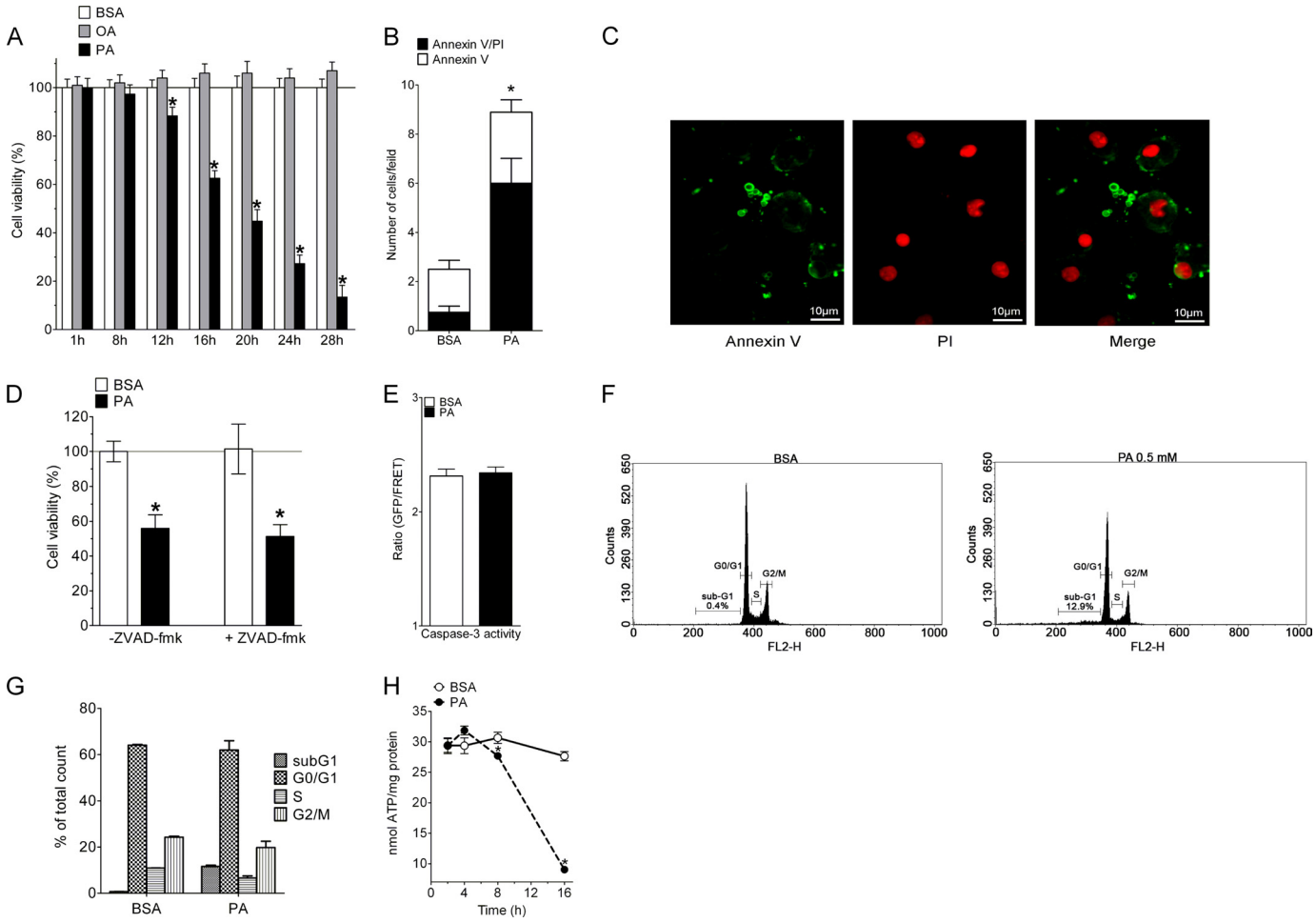

FIGURE 1. **PA induces necrotic cell death in endothelial cells.** *A*, cells were treated with BSA alone (*white columns*, $n = 3$), 0.5 mM OA (*gray columns*, $n = 3$), or 0.5 mM PA (*black columns*, $n = 3$) and cell viability was measured with MTT assay at the time points indicated. Fatty acids were complexed to BSA. Data were normalized to BSA as control and represented as percentage viability. *, $p < 0.05$ *versus* BSA. *B*, annexin V/PI costaining for the cells exposed to 0.5 mM PA ($n = 4$) or BSA alone ($n = 4$) (*asterisk* refers to annexin V/PI). *, $p < 0.05$ *versus* BSA. *C*, representative images of annexin V/PI-stained endothelial cells treated with 0.5 mM PA for 12 h ($n = 4$). Images were taken using a ×40 objective. *D*, cells were treated with the solvent (DMSO, control, -Z-VAD-fmk, $n = 3$) or with 20 μM Z-VAD-fmk (+*zVAD-fmk*, $n = 3$) prior to treatment with 0.5 mM PA or BSA alone and cellular viability was measured with MTT assay. *, $p < 0.05$ *versus* BSA (51.3 ± 6.7% in the Z-VAD-fmk treated as compared with 55.9 ± 7.7% in controls). *E*, caspase-3 activity measured with the FRET-based sensor Casper 3-GR, expressed as ratio GFP/FRET of randomly selected cells under control conditions (BSA, *white column*, $n = 3$, 81 cells) and after cell treatment with 0.5 mM PA for 16–18 h ($n = 3$, 102 cells). *F*, histograms of cell cycle analysis by flow cytometry for DNA hypoploidy. Cells were treated with BSA or 0.5 mM PA and were analyzed after 18 h of incubation. *G*, statistical analysis of the histograms shown in *panel F*. *H*, statistical data representing nmol of ATP/mg of protein in the cells exposed to 0.5 mM PA (*black circles*, *dotted line*, $n = 6$ for each time point) or BSA alone (*white circles*, *continuous line*, $n = 6$ for each time point). *, $p < 0.05$ *versus* BSA.

the MTT assay at different times of incubation (Fig. 1*A*). After 12 h of incubation with PA, cell viability was found to be already significantly reduced and further decreased with time. The cell viability declined more than 80% after 28 h of incubation with PA (Fig. 1*A*), pointing to a strong cytotoxic effect of this saturated fatty acid on endothelial cells. The PA-induced cell death was further examined using long-term phase-contrast imaging, which showed an impaired cell proliferation and an accumulation of detached, dying cells upon incubation with PA (supplemental Fig. S1 and Movie S1). In contrast, cell treatment with OA did not affect the viability of the cells (Fig. 1*A*). These findings are in line with earlier studies using other cell types (26) and approved EA.hy926 cells as a suitable model to explore the molecular mechanisms of PA-mediated lipotoxicity.

Next, the mode of PA-induced cell death was investigated by annexin V and PI staining. A major proportion of the cells exposed to PA for 12 h were found to be positive both for annexin V and PI (Fig. 1, *B* and 1*C*), which is indicative of necrosis. Moreover, the annexin V/PI-positive cells contained round and intact nuclei (Fig. 1*C*), pointing to necrotic cell death. To further exclude the role of apoptosis in the process of PA-induced death of the endothelial cells, cells were treated with benzyloxycarbonyl-Val-Ala-Asp(OMe)-fluoromethylketone (Z-VAD-fmk), a cell permeable, irreversible pan-caspase inhibitor that hinders apoptosis (27). Z-VAD-fmk failed to exhibit any effect on PA-induced endothelial cell death (Fig. 1*D*), thus, further confirming that the mode of PA-induced death of the endothelial cells was necrotic and not apoptotic. The absence of caspase activation in PA-induced cell death was further documented using the caspase-3 apoptosis sensor Casper3-GR (24). Casper3-GR is a FRET-based sensor for measuring caspase-3 activity, consisting of a green (GFP) and a RFP that are connected by the caspase-3 cleavage sequence DEVD (supplemental Fig. S2*A*). As a positive control cells expressing Casper3-GR were treated with staurosporine, which revealed a strong increase of the GFP/FRET ratio after 80 min, indicating the cleavage of the

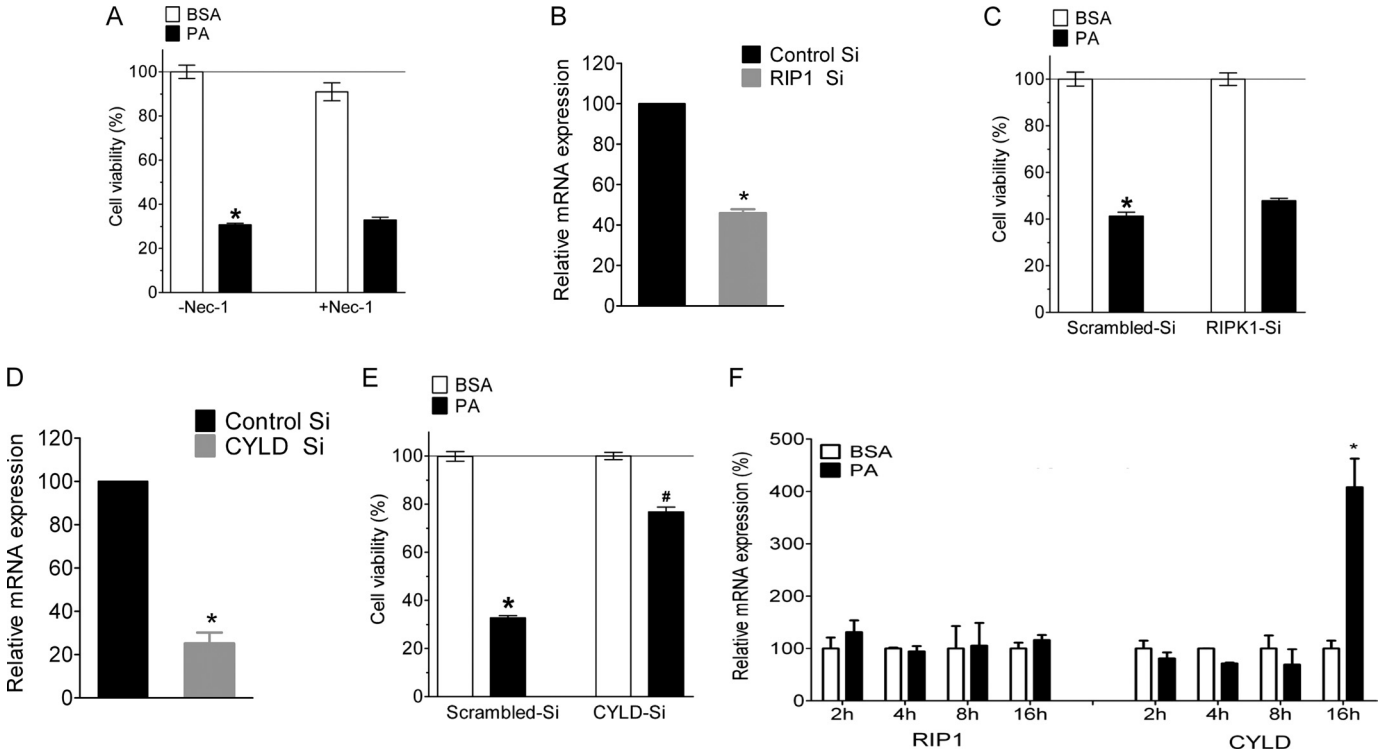

FIGURE 2. **PA induces RIPK1 independent but CYLD dependent necroptosis in endothelial cells.** *A*, cells were pretreated with solvent (DMSO, control, -Nec-1, $n = 4$) or 30 μM necrostatin-1 (+*Nec-1*, $n = 4$) for 20 min and were incubated for 24 h with BSA or 0.5 mM PA and cellular viability was measured with MTT assay. *, $p < 0.05$ *versus* BSA. *B*, knockdown efficiency of RIPK1 (*RIP1*) siRNA in the percentage of mRNA expression compared with scramble siRNA ($n = 3$ for all columns presented). *, $p < 0.05$ *versus* scrambled siRNA. *C*, cell viability 48 h after transfection of cells with either scrambled siRNA (*left pair* of columns, $n = 18$ for both conditions) or siRNA against RIPK1 (*right pair* of columns, $n = 18$ for both conditions). Cells were incubated for 24 h with BSA alone (*white columns*) or 0.5 mM PA complexed to BSA (*black columns*) and cell viability was measured using the MTT assay. Viability is expressed in percentage, whereas the average value of cells treated with scrambled siRNA and BSA alone was defined as 100%. *, $p < 0.05$ *versus* BSA, and #, $p < 0.05$ *versus* PA with scrambled siRNA (47.8 ± 1.0% dead cells in RIPK1-siRNA as compared with 41.2 ± 1.6% dead cells in scrambled siRNA). *D*, knockdown efficiency of CYLD siRNA in percentage of mRNA expression compared with scramble siRNA ($n = 6$). *, $p < 0.05$ *versus* scrambled siRNA. At 16 h more than 40% of the cells were found dead by the MTT assay as shown in Fig. 1*A*. *E*, impact of siRNA-mediated knockdown of CYLD on cell viability under analogous conditions described in *panel C* ($n = 18$ for each column). *, $p < 0.05$ *versus* BSA, and #, $p < 0.05$ *versus* PA with scrambled siRNA. *F*, the relative mRNA expression of RIPK1 and CYLD in cells treated with BSA or 0.5 mM PA for 2, 4, 8, and 16 h. The relative expression is presented as a percentage of BSA-treated cells at the given time point. *, $p < 0.05$ *versus* BSA at the given time point ($n = 3$).

sensor by the activation of caspase-3 (supplemental Fig. S2, *B* and *C*). In contrast, cell treatment with PA for 16 h failed to increase the basal GFP/FRET ratio of Casper3-GR, indicating the absence of caspase-3 activation (Fig. 1*D* and supplemental Fig. 2*D*). Moreover, the quantification of DNA hypoploidy by FACS showed only a small proportion of cells with reduced DNA content when cells were treated with PA for 18 h (Fig. 1, *F* and *G*). In line with these findings PA did not induce DNA laddering even if cells were treated for 24 h with the fatty acid (supplemental Fig. S2*E*), whereas under these conditions 70% of the cells were found dead with the MTT assay. In summary, these data confirm that the PA-induced cell death is predominantly necrotic.

In line with these findings, HPLC analysis revealed significantly reduced ATP levels in cells that have been exposed to PA already at 8 h and further decreased tremendously until 16 h (Fig. 1*H*), emphasizing necrosis as the terminal point of PA-induced cell damage. As the onset of cell death is between the 8- and 16-h time point the drop in ATP levels are earlier than the onset of cell death and more than 40% of the cells were already found dead after 16 h as indicated in Fig. 1*A*. These data challenge the dogma that lipotoxicity is exclusively apoptotic and align with our earlier findings that free fatty acids induce necrosis and not apoptosis in yeast (7).

PA Induces RIPK3 and CYLD-dependent but RIPK1-independent Programmed Necrosis (Necroptosis)—Evidence has accumulated that the necrotic pathway can also occur in a highly regulated manner (28). Particularly the kinases receptor-interacting protein kinase-1 (RIPK1), RIPK3, and the receptor interacting protein (RIP) 1 de-ubiquitin enzyme CYLD are known initiators of programmed necrosis, a cell death pathway, which is also referred to as necroptosis (29, 30). Accordingly, we next investigated the molecular mechanism of PA-induced necrosis in endothelial cells. For this purpose we first used necrostatin-1, a specific inhibitor for RIPK1. As represented in Fig. 2*A* necrostatin-1 did not affect the PA-induced cell death. In line with this finding siRNA-mediated knockdown of RIPK1 (Fig. 2*B*) could not inhibit PA-induced cell death (Fig. 2*C*). On the other hand a knockdown of CYLD (Fig. 2*D*) could inhibit the PA-induced cell death significantly (Fig. 2*E*). In line with these results we unveiled strong elevation of the mRNA level of CYLD after 16 h of incubation with PA, whereas no change in the expression pattern of RIPK1 could be observed under these conditions (Fig. 2*F*). We failed to perform respective experi-

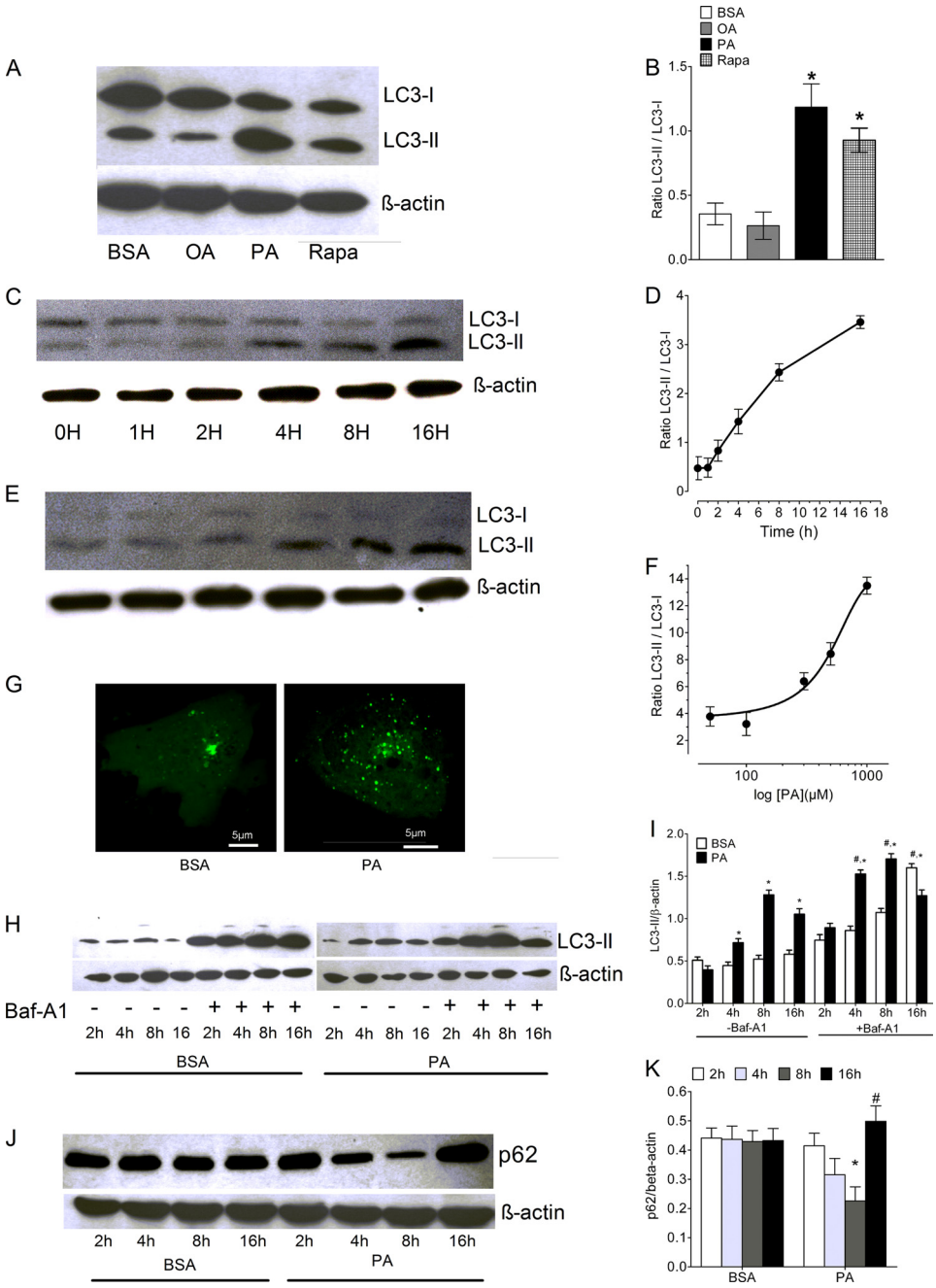

FIGURE 3. **PA induces autophagy in endothelial cells.** *A*, cells were treated with BSA, OA, PA, and rapamycine (*Rapa*) for 8 h and the extracted protein was immunoblotted against LC3 antibody. *β*-Actin was used to normalize the data for equal protein loading. *B*, *columns* represent the average band densities from 3 different experiments as shown in *panel A*. *, $p < 0.05$ *versus* BSA. *C* and *D*, time dependence of the PA-induced cleavage of LC3 expressed as the LC3-II/LC3-I ratio over time ($n = 3$ for each time point). *E* and *F*, concentration-response curve of PA-induced cleavage of LC3 ($n = 3$ for each concentration). PA was complexed to BSA. *G*, representative images of cells expressing Venus-LC3. Images show the subcellular distribution of Venus-LC3 in control cells (*left image*, BSA alone for 8 h after cell transfection) and in cells treated for 8 h with 0.5 mM PA complexed to BSA (*right image*). *H*, cell were treated with BSA or 0.5 mM PA in the presence or absence of bafilomycin A1 (*Baf-A1*) and the isolated proteins at the given time points were immunoblotted for LC3. Representative image of three independent experiments is presented, whereas statistical data of three independent experiments are shown in *panel I*. *, $p < 0.05$ *versus* BSA at a given time point, and #, $p < 0.05$ *versus* PA with treated with DMSO (control, *-Baf-A1*) at a given time point ($n = 3$). *J*, a representative image of three independent experiments showing the degradation pattern of p62. Cells were treated with BSA or 0.5 mM PA and isolated proteins at the given time points were blotted for p62. Statistical data of three independent experiments are shown in *panel K*). *, $p < 0.05$ *versus* BSA at a given time point; #, $p < 0.05$ *versus* PA at 8-h time point ($n = 3$).

ments for RIPK3 expression levels most likely because of too low mRNA levels coding for this protein in the endothelial cells used (supplemental Fig. 4, *A* and *B*). Nevertheless, cells treated with a validated siRNA against RIPK3 (29) showed a significantly increased viability if treated with PA for 24 h in four sets of independent experiments (supplemental Fig. S4*C*). Although we could not quantify the RIPK3 knockdown efficiency these findings suggest that PA induces a CYLD- and RIPK3-dependent but RIPK1-independent programmed necrosis.

PA Triggers Autophagy in Endothelial Cells—Recent data demonstrated the induction of autophagy by PA in beta cells (8). Accordingly, a possible role of autophagy in PA-induced

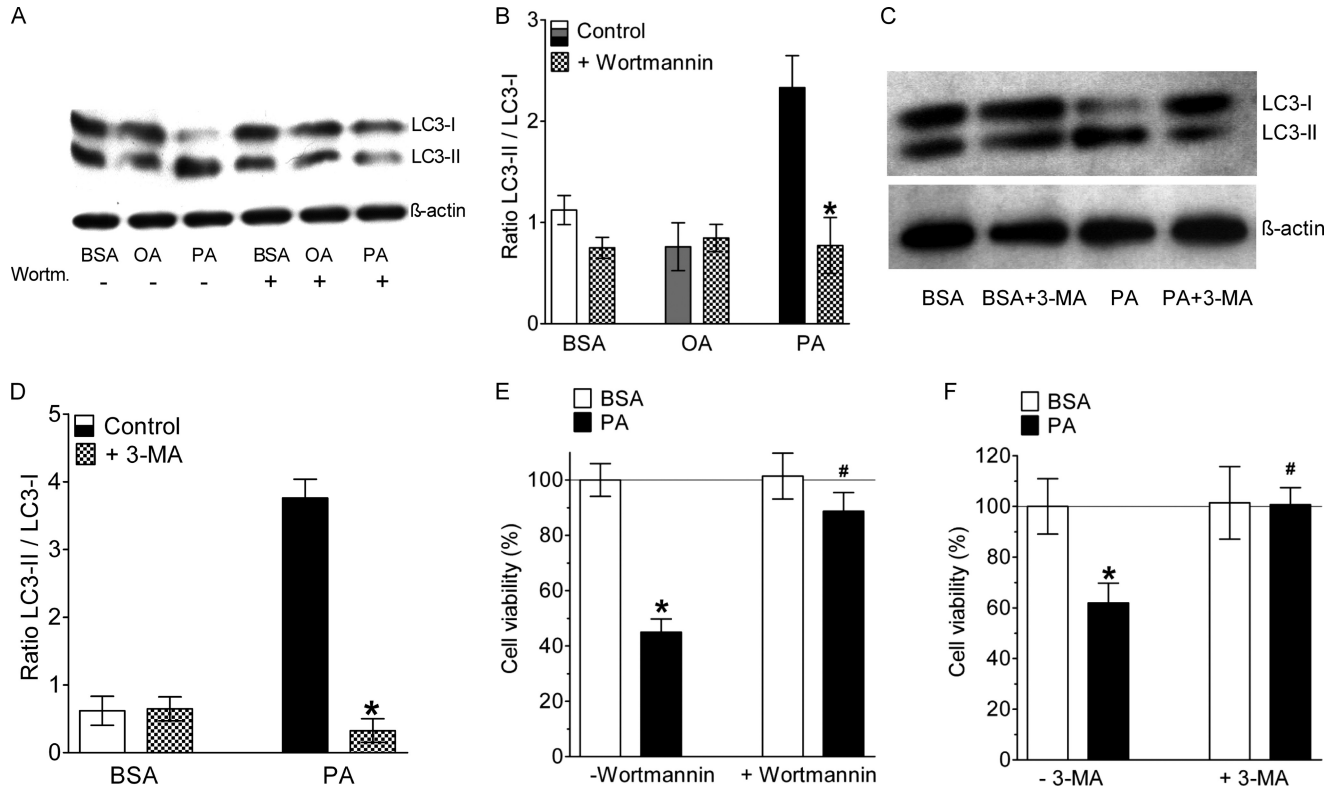

FIGURE 4. **Inhibition of autophagy rescued endothelial cells from PA-induced death.** *A*, representative Western blot showing LC3 cleavage of cells that were incubated for 8 h with BSA alone, 0.5 mM OA, or 0.5 mM PA in the absence (−) and presence (+) of 10 μM wortmannin. *B,* statistical data of LC3 cleavage from Western blots shown in *panel f* ($n = 3$ for all conditions). *, $p < 0.05$ *versus* control. *C*, representative Western blot showing LC3 cleavage of cells that were incubated for 8 h with BSA alone or 0.5 mM PA in the absence (−) and presence (+) of 10 mM 3-MA. *D*, statistical data of LC3 cleavage from Western blots shown in *panel f* ($n = 3$ for all conditions). *, $p < 0.05$ *versus* control. *E*, columns represent average cell viabilities that were determined using the MTT assay of cells not pretreated with wortmannin (*left pair* of columns, −*Wortmannin*) that were incubated for 24 h with BSA alone (*left white column*, $n = 3$) or with 0.5 mM PA complexed to BSA (*left black column*, $n = 3$), and cells pretreated with 10 μM wortmannin (*right pair of columns*, +*Wortmannin*) for 20 min prior to an incubation with either BSA alone (*right white column*, $n = 3$) or with 0.5 mM PA complexed to BSA (*right black column*, $n = 3$). *, $p < 0.05$ *versus* BSA, and #, $p < 0.05$ *versus* PA without wortmannin. *F*, cells were treated with 10 mM 3-MA, another specific inhibitor of PI3K III and autophagy, and cell death was analyzed by the MTT assay ($n = 3$ for all conditions). *, $p < 0.05$ *versus* BSA, and #, $p < 0.05$ *versus* PA without 3-MA.

cell death was investigated. For this purpose cleavage of the microtubule-associated protein 1 light chain 3 (LC3), a marker for autophagy (31), was blotted. Considerable cleavage and lipidation of LC3 to LC3-I (not lipidated) and the phosphatidylethanolamine-conjugated LC3-II was detected in cells that were treated with PA, whereas OA did not induce LC3-II formation (Fig. 3, *A* and *B*). To gauge the magnitude of the induction of autophagy by PA, cells were also treated with 50 nM rapamycin, a well characterized inducer of autophagy (32). As shown in Fig. 3, *A* and *B,* PA was even more effective than rapamycin to stimulate LC3-II formation under these conditions. The PA-induced conversion of LC3-I to LC3-II depended on both the time of PA incubation (Fig. 3, *C* and *D*) and the concentration of the fatty acid (Fig. 3, *E* and *F*). The induction of autophagy by PA was further examined by imaging the cellular distribution of Venus-LC3, a fusion construct of the yellow fluorescent protein Venus with LC3. In control cells that were treated with BSA alone Venus-LC3 was mainly distributed in the cytosol and only a small number of autophagosomes were visible, indicating a low level of autophagy under these conditions (Fig. 3*G*, *left panel*). In contrast, cells incubated with PA for 8 h exhibited a large number of autophagosomes with accumulated Venus-LC3 (presumably as Venus-LC3-II). This confirms the induction of autophagy by PA in the EA.hy926 cells (Fig. 3*G*, *right panel*).

To verify whether or not the PA-induced autophagy goes to completion, we measured LC3-II also in the presence of bafilomycin A (50 nM), a known inhibitor of the autophagic flux (32). As shown in Fig. 3, *H* and *I,* LC3-II was further increased in the presence of bafilomycin A under control conditions and in cells pretreated with PA until 8 h. These findings indicated that PA is a genuine and strong inducer of autophagy in endothelial cells. However, at 16 h of incubation with PA the accumulation of LC3-II was hampered, indicating the onset of incomplete autophagy. This finding was further supported by the degradation pattern of sequestome 1 (p62), a frequently used marker for the measurement of the autophagic flux (32). Corresponding to the pattern of LC3-II accumulation (Fig. 3, *H* and *I*), the levels of p62 gradually decreased in cells treated with PA until 8 h, whereas a significant accumulation of this protein was observed at 16 h (Fig. 3, *J* and *K*).

Inhibition of Autophagy Rescues Endothelial Cells from PA-induced Cell Death—To investigate the role of autophagy induction on cell death we inhibited autophagy with wortmannin or 3-MA and measured the effect on lipotoxic cell death. Wortmannin and 3-MA are known to prevent autophagy by

their inhibitory effect on VPS34 (33, 34). As expected, inhibition of VPS34 by either wortmannin prevented PA-induced autophagy indicated by a lack of LC3 cleavage in cells pretreated with this inhibitor (Fig. 4, *A–D*).

Hence, we investigated the putative role of autophagy on lipotoxic cell death. We found that the cells pretreated with wortmannin were resistant to PA-induced cell death even after 36 h of incubation with the fatty acid (Fig. 4*E*). As wortmannin inhibits all different classes of PI3Ks, the effect of 3-MA, a highly specific inhibitor of PI3K class III (vesicular protein sorting 34; VPS34) was tested. As shown in Fig. 4*F*, 3-MA was also highly effective in preventing PA-induced cell death. The effect of PI3K (class III) inhibitors on PA-induced cell death was further tested using long-term phase-contrast microscopy, which confirmed their potency to rescue endothelial cells from PA-mediated lipotocixity (supplemental Fig. S3 and Movie S2).

Genetic Knockdown of Autophagy Related Genes Rescues PA-induced Cell Death—To further confirm the role of autophagy in the cell death process we knocked-down VPS34 and ATG7, two autophagy-specific proteins and the effects thereof on PA-induced cell death were investigated. The siRNAs against both VPS34 and ATG7 were efficient in decreasing respective mRNA levels (Fig. 5*A*). Knockdown of either VPS34 or ATG7 strongly reduced PA-induced endothelial cell death (Fig. 5, *B* and *C*).

PA-induced Ca^{2+} Elevation Triggers Autophagy in Endothelial Cells—Recently there are some reports about the role of Ca^{2+} in autophagy (35). We chelated cytosolic Ca^{2+} with BAPTA-AM and measured the cleavage of LC3 by Western blotting. It was found that autophagy was inhibited by BAPTA-AM treatment (Fig. 6, *A* and *B*). This indicated that the induction of autophagy by PA was dependent on cytosolic Ca^{2+} elevation.

To verify whether or not cell treatment with PA impacts Ca^{2+} signaling of endothelial cells we measured cytosolic Ca^{2+} under the conditions of fatty acid exposure. Basal $[Ca^{2+}]_{cyto}$ was assessed first in the presence and absence of extracellular Ca^{2+} using Fura-2/AM-loaded cells. Subsequently, Ca^{2+} was released from the endoplasmic reticulum (ER) in a Ca^{2+}-free medium by cell stimulation with the IP_3-generating agonist histamine and the sarco/endoplasmic reticulum Ca^{2+}-ATPase inhibitor BHQ to assess the ER Ca^{2+} content (Fig. 6*C*). In a Ca^{2+}-containing buffer the treatment with PA caused a significant increase of basal levels of $[Ca^{2+}]_{cyto}$ already after 4 h of incubation, and $[Ca^{2+}]_{cyto}$ remained elevated until 8 and 16 h of incubation (Fig. 6, *D* and *E*). Removal of extracellular Ca^{2+} led to a decrease in basal $[Ca^{2+}]_{cyto}$ in cells that were pretreated with PA, indicating that store-operated Ca^{2+} entry was activated (Fig. 6*C*). In contrast, cells incubated with OA did not show significant changes of basal Ca^{2+} levels in the cytosol (Fig. 6, *C* and *D*). The amount of releasable Ca^{2+} from the ER was clearly smaller in cells pretreated with PA (Fig. 6, *C* and *E*). Notably, the effect on ER Ca^{2+} mobilization was seen already after a 2-h incubation with PA and was more pronounced with time (Fig. 6*E*). Cells pretreated with OA, however, revealed normal Ca^{2+} signals upon ER Ca^{2+} depletion (Fig. 6, *C* and *E*). These data indicate that the accumulation of PA within endothelial cells is associated with a slow, time-dependent leak of

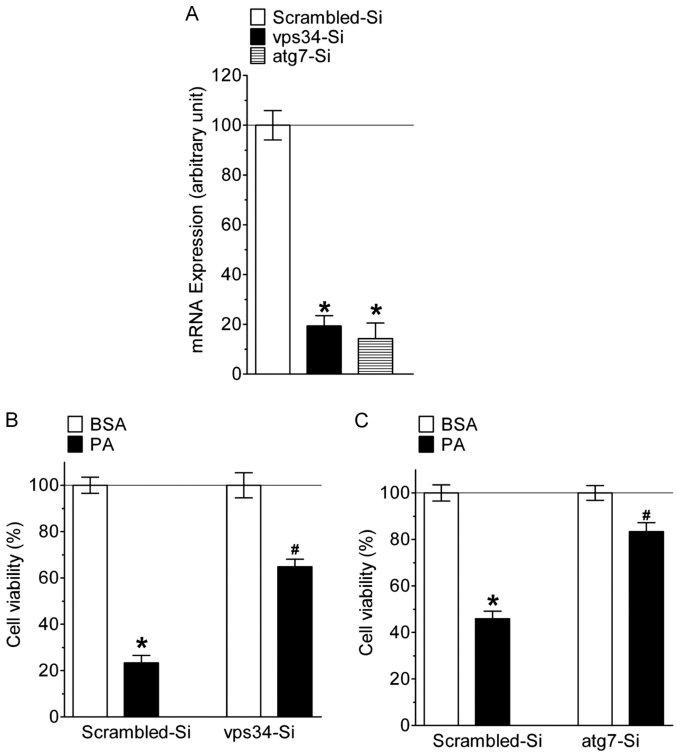

FIGURE 5. **Genetic knockdown of autophagy specific genes rescued cells from PA-induced cell death.** *A*, knockdown efficiency of individual siRNA in the percentage of mRNA expression compared with scramble siRNA ($n = 3$ for all columns presented). *, $p < 0.05$ *versus* scrambled siRNA. *B*, 48 h after cells transfection with either scrambled siRNA (*left pair of columns*, $n = 9$ for both conditions) or siRNA against VPS34 (*right pair of columns*, $n = 9$ for both conditions) cells were incubated for 24 h with BSA alone (*white columns*) or 0.5 mM PA complexed to BSA (*black columns*) and cell viability was measured using the MTT assay. Viability is expressed in percentage, whereas the average value of cells treated with scrambled siRNA and BSA alone was defined as 100%. *, $p < 0.05$ *versus* BSA, and #, $p < 0.05$ *versus* PA with scrambled siRNA. *C*, impact of siRNA-mediated knockdown of ATG7 on cell viability under analogous conditions described in *panel b* ($n = 9$ for each column). *, $p < 0.05$ *versus* BSA, and #, $p < 0.05$ *versus* PA with scrambled siRNA.

Ca^{2+} from the ER. The consequence is a reduced Ca^{2+} content of the ER and elevated basal cytosolic Ca^{2+} levels, possibly due to the stimulation of Ca^{2+} entry via the store-operated Ca^{2+} entry pathway.

Furthermore, we investigated the role of cytosolic Ca^{2+} on cell viability. Cells were treated with BAPTA-AM for 20 min prior to treatment with PA for 24 h, and cellular viability was measured with the MTT assay. It was found that cell loading with BAPTA-AM inhibited PA-induced cell death significantly (Fig. 6*F*).

DISCUSSION

Herein we provide evidence that exposure of endothelial cells to pathological PA concentrations generates a lipotoxic response that finally leads to necrotic cell death. The lethal effect of PA is initially triggered by the development of Ca^{2+} leakage of the ER, which leads to elevated basal cytosolic Ca^{2+}. Subsequently, the initiation of Ca^{2+}-dependent autophagy turns to be harmful to the cells leading to RIPK3- and CYLD-dependent necrotic cell death. These data unveil a so far unknown pathway of lipotoxicity and point to ER Ca^{2+} leakage, Ca^{2+}-dependent autophagy, and programmed necrosis as a hallmark of lipotoxicity in endothelial cells.

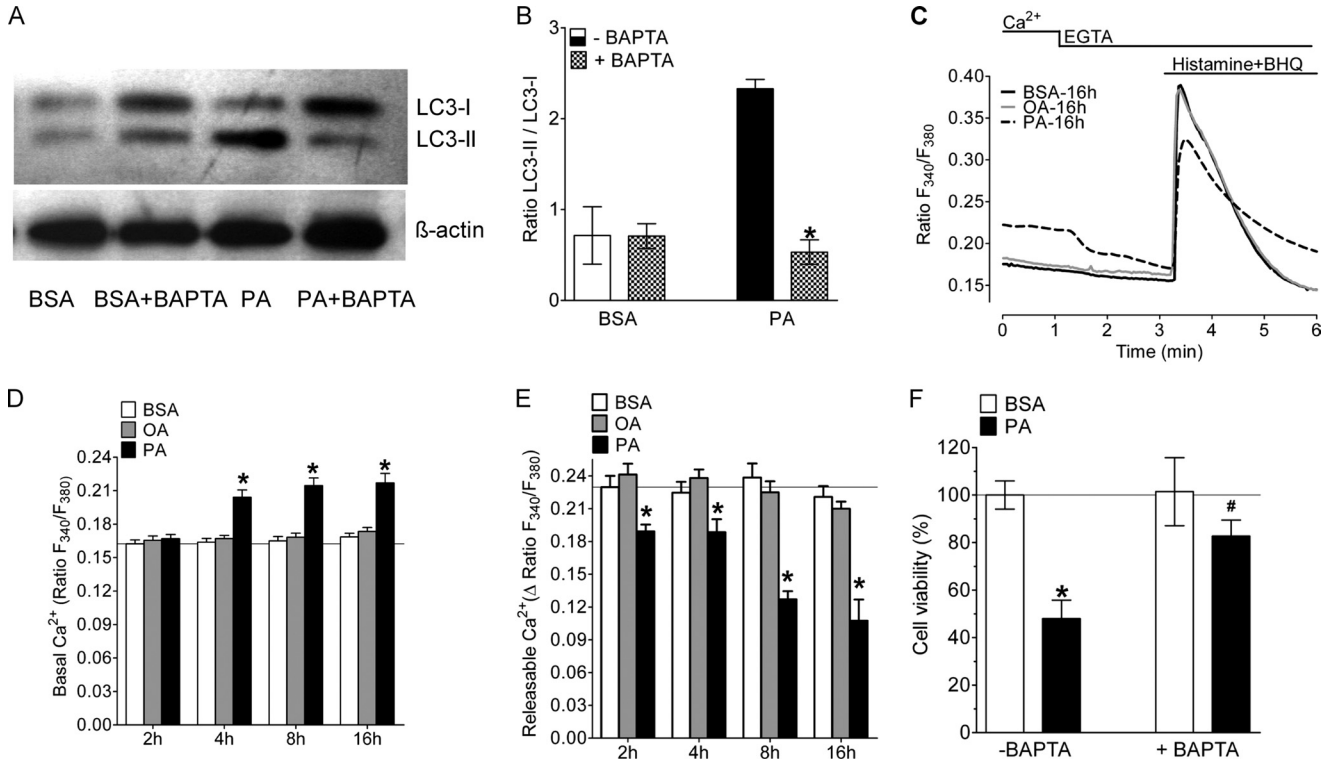

FIGURE 6. **PA-induced autophagy and cell death is a Ca^{2+}-dependent process.** *A,* representative Western blot showing LC3 cleavage of BAPTA-AM-loaded cells that were incubated for 8 h with BSA alone or 0.5 mM PA. *B,* statistical data of LC3 cleavage from Western blots ($n = 3$ for all conditions). *, $p < 0.05$ *versus* control. PA induces release of Ca^{2+} from ER and results in cytosolic Ca^{2+} elevation. *C,* representative Ca^{2+} signals of Fura-2/AM-loaded cells 16 h after incubation with BSA alone (*black continuous line*), 0.5 mM OA (*gray continuous line*), and 0.5 mM PA (*black dotted line*). The indicated signals were first recorded in Ca^{2+} containing medium (2 mM) and subsequently Ca^{2+} was mobilized from the ER by cell stimulation with 100 μM histamine and 15 μM BHQ in a Ca^{2+}-free medium (1 mM EGTA). *D,* statistics of basal ratio values of Fura-2/AM-loaded cells in the presence of extracellular Ca^{2+} (2 mM), and *E,* average δ values of the maximal Ca^{2+} peaks upon cell stimulation with 100 μM histamine and 15 μM BHQ in the absence of extracellular Ca^{2+} (1 mM EGTA) at different times after incubation with BSA alone (Control, *white columns*, $n = 9$, ×118 cells at 2 h, ×127 cells at 4 h, ×130 cells at 8 h, and ×127 cells at 16 h), with 0.5 mM OA (*gray columns*, $n = 9$, ×113 cells at 2 h, ×127 cells at 4 h, ×133 cells at 8 h, and ×132 cells at 16 h), and with 0.5 mM PA (*black columns*, $n = 9$, ×115 cells at 2 h, ×124 cells at 4 h, ×118 cells at 8 h and ×107 cells at 16 h). *, $p < 0.05$ *versus* BSA. *F,* effect of chelating cytosolic Ca^{2+} on cell viability. Cells were pretreated with BAPTA-AM for 20 min and then incubated with 0.5 mM PA or BSA alone for 24 h. Cell viability was measured with the MTT assay and data were normalized to BSA as a control and represented as mean viability ($n = 3$, for all conditions). *, $p < 0.05$ *versus* BSA, and #, $p < 0.05$ *versus* PA without BAPTA-AM-loaded cells.

PA Induces Programmed Necrosis of Endothelial Cells—Although it has been reported that apoptosis is the major executer of cell death under conditions of substrate overload (26), our data clearly indicate that an overload of endothelial cells with PA causes necrosis. We used Z-VAD-fmk to rule out the contribution of pan-caspases in the execution of PA-induced cell death. However, this set of experiments might also point to caspase-independent apoptosis in the cell model used (36). Nevertheless, our findings that cells treated with PA were positive for both annexin V and PI, did not show caspase activity, and the early depletion of ATP strongly indicates necrotic cell death. Moreover, only a small fraction (11.6%) of cells treated with PA showed DNA hypoploidy, indicating that necrosis is the predominant mode of cell death. On the other hand these experiments, which were performed with the whole cell population (*i.e.* attached and floating cells), might point to a mixture of apoptosis and necrosis. Nevertheless, the reduced energy supply might rather explain the necrotic mode of cell death, as it has been reported that ATP levels determine the mode of cell death (37).

In addition, the nuclear morphology of cells challenged with toxic concentrations of PA supported the necrotic cell death. The dying endothelial cells contained round and intact nuclei, and no nuclear fragmentation, which typically occurs during apoptosis (38), was observed.

In addition, a knockdown of the known players of programmed necrosis, RIPK3 (29) and CYLD (30), rescued the cells from PA-induced cell death. Although we could not detect RIPK3 mRNA levels in control cells and cells treated with PA for 16 h we were successful in inhibiting the PA-induced cell death by using a previously reported siRNA against RIPK3 (29). The rescuing effect of a siRNA-mediated knockdown of RIPK3 was less pronounced compared with that of a CYLD knockdown, but reproducible and significant. We concluded that mRNA levels coding for RIPK3 are too low to be specifically detected and quantified, possibly also because of a low stability of the respective mRNA in the preparations used. Although we cannot exclude any off target effects of the validated siRNA (29) used to knockdown RIPK3 in endothelial cells, the functional tests clearly suggested an involvement of this kinase in the toxic signaling of PA. Interestingly, our data also unveiled that PA triggers the expression of CYLD, whereas the molecular mechanisms involved have not been clarified so far. This finding supports the assumption that a necrotic pathway is induced by PA in endothelial cells. RIPK1 is another known player of programmed necrosis, however, siRNA-mediated knockdown of

RIPK1 as well as the usage of necrostatin-1 indicated that RIPK1 does not contribute to the PA-induced necroptosis in this particular endothelial cell line. This finding is in line with recent reports, in which a RIPK1-independent but RIPK3- and CYLD-dependent cell death pathway has been described (39, 40). The induction of RIPK3- and CYLD-dependent necroptosis by PA described here may, however, point to novel strategies for the treatment of metabolic diseases.

PA Induces Autophagy, Which Promotes Cell Death—Recently there are reports about the induction of autophagy by free fatty acid in different cell types (8, 41, 42). This is in line with our finding showing that PA initiates enhanced autophagy in the endothelial cells used. However, in contrast to our findings it was shown in pancreatic beta cells that the induction of autophagy was a pro-survival mechanism and inhibiting autophagy with pharmacological inhibitors enhanced the cell death (8). In contrast, our findings demonstrate that autophagy is the main trigger of PA-induced cell death, as the inhibition of autophagy with either pharmacological inhibitors or genetic knockdown could rescue the cells from PA-induced cell death. At a first glance this is in line with recent reports that describe autophagy as a mechanism able to induce type II programmed cell death (15, 43). Autophagy can contribute to cell death, particularly if the process is hampered by lysosomal dysfunction (44). We did not test whether or not endothelial cells develop lysosomal dysfunction in response to PA. However, in recent reports PA was shown to induce lysosomal dysfunction in PC12 and pancreatic beta cells. Notably, PA was found to suppress autophagic turnover in beta cells leading to lower ATP levels. Our finding regarding the ATP depletion in endothelial cells treated with PA is in line with this report. Moreover, we could see clear signs of a hampered autophagic flux at 16 h of cell treatment with PA. Hence, it is tempting to speculate that PA might cause a parallel lysosomal dysfunction resulting in depletion of ATP, which ultimately leads to necrosis of the endothelial cells used.

PA Affects ER Ca^{2+} Storage—Although the detailed mechanisms that induce ER Ca^{2+} mobilization by PA leading to elevated cytosolic Ca^{2+} remain unclear our data indicate that this is an early and central process of PA-induced cell damage. We did not observe an acute effect of PA on the Ca^{2+} homeostasis of endothelial cells, indicating that the accumulation of PA, its metabolism or derivates might be responsible for developing aberrant Ca^{2+} signals in endothelial cells. The finding that cells treated with PA had a lower ER Ca^{2+} content and increased levels of $[Ca^{2+}]_{cyto}$ is in line with a recent report that describes ER Ca^{2+} release by PA in beta cells (45). Ca^{2+} signaling is known to be involved in all types of cell death (46) and also plays a fundamental role in the induction of ER stress (47) and autophagy (35). Our finding that cytosolic Ca^{2+} chelation by BAPTA protected the cells against PA-induced death is of particular relevance, because it points to a possibility of a therapeutic intervention against lipotoxicity.

In summary our study describes that PA overload of endothelial cells results in a Ca^{2+}-dependent development of autophagy, which finally lead to programmed necrotic cell death. This molecular mechanism of lipotoxicity reported herein enlightens a new mechanism of lipotoxic cell death of endothelial cells and might guide to novel strategies in the therapy of vascular diseases that are caused by the accumulation of fatty acids in endothelial cells.

Acknowledgments—We thank Anna Schreilechner, Florian Enzinger, and Rene Rost for excellent technical assistance and Dr. C. J. S. Edgell (University of North Carolina, Chapel Hill, NC) for the EA.hy926 cells.

REFERENCES

1. Brookheart, R. T., Michel, C. I., and Schaffer, J. E. (2009) As a matter of fat. *Cell Metab.* **10,** 9–12
2. Unger, R., and Zhou, Y. (2001) Lipotoxicity of beta cells in obesity and in other causes of fatty acid spillover. *Diabetes* **1,** S118–S121
3. Borradaile, N. M., and Schaffer, J. E. (2005) Lipotoxicity in the heart. *Curr. Hypertens. Rep.* **7,** 412–417
4. Pfaffenbach, K. T., Gentile, C. L., Nivala, A. M., Wang, D., Wei, Y., and Pagliassotti, M. J. (2010) Linking endoplasmic reticulum stress to cell death in hepatocytes. Roles of C/EBP homologous protein and chemical chaperones in palmitate-mediated cell death. *Am. J. Physiol. Endocrinol. Metab.* **298,** E1027–E1035
5. Mayer, C. M., and Belsham, D. D. (2010) Palmitate attenuates insulin signaling and induces endoplasmic reticulum stress and apoptosis in hypothalamic neurons. Rescue of resistance and apoptosis through adenosine 5′-monophosphate-activated protein kinase activation. *Endocrinology.* **151,** 576–585
6. Meyers, M. R., and Gokce, N. (2007) Endothelial dysfunction in obesity. Etiological role in atherosclerosis. *Curr. Opin. Endocrinol. Diabetes Obes.* **14,** 365–369
7. Rockenfeller, P., Ring, J., Muschett, V., Beranek, A., Buettner, S., and Carmona-Gutierrez, D., Eisenberg, T., Khoury, C., Rechberger, G., Kohlwein, S. D., Kroemer, G., and Madeo, F. (2010) Fatty acids trigger mitochondrion-dependent necrosis. *Cell Cycle* **9,** 2836–2842
8. Choi, S. E., Lee, S. M., Lee, Y. J., Li, L. J., Lee, S. J., Lee, J. H., Kim, Y., Jun, H. S., Lee, K. W., and Kang, Y. (2009) Protective role of autophagy in palmitate-induced INS-1 beta cell death. *Endocrinology* **150,** 126–134
9. Almaguel, F. G., Liu, J. W., Pacheco, F. J., De Leon, D., Casiano, C. A., and De Leon, M. (2010) Lipotoxicity-mediated cell dysfunction and death involve lysosomal membrane permeabilization and cathepsin L activity. *Brain Res.* **1318,** 133–143
10. Kristensen, A. R., Schandorff, S., Høyer-Hansen, M., Nielsen, M. O., Jäättelä, M., Dengjel, J., and Andersen, J. S. (2008) Ordered organelle degradation during starvation-induced autophagy. *Mol. Cell Proteomics* **7,** 2419–2428
11. Scherz-Shouval, R., and Elazar, Z. (2007) ROS, mitochondria and the regulation of autophagy. *Trends Cell Biol.* **17,** 422–427
12. Galluzzi, L., Vitale, I., Abrams, J. M., Alnemri, E. S., Baehrecke, E. H., Blagosklonny, M., Dawson, T. M., Dawson, V. L., El-Deiry, W. S., Fulda, S., Gottlieb, E., Green, D. R., Hengartner, M. O., Kepp, O., Knight, R. A., Kumar, S., Lipton, S. A., Lu, X., Madeo, F., Malorni, W., Mehlen, P., Nuñez, G., Peter, M. E., Piacentini, M., Rubinsztein, D. C., Shi, Y., Simon, H. U., Vandenabeele, P., White, E., Yuan, J., Zhivotovsky, B., Melino, G., and Kroemer, G. (2012) Molecular definitions of cell death subroutines. Recommendations of the Nomenclature Committee on Cell Death 2012. *Cell Death Differ.* **19,** 107–120
13. Yuan, J., and Kroemer, G. (2010) Alternative cell death mechanisms in development and beyond. *Genes Dev.* **24,** 2592–2602
14. Samara, C., Syntichaki, P., and Tavernarakis, N. (2008) Autophagy is required for necrotic cell death in *Caenorhabditis elegans*. *Cell Death Differ.* **15,** 105–112
15. Levine, B., and Yuan, J. (2005) Autophagy in cell death. An innocent convict? *J. Clin. Invest.* **115,** 2679–2688
16. Espert, L., Denizot, M., Grimaldi, M., Robert-Hebmann, V., Gay, B., Varbanov, M., Codogno, P., Biard-Piechaczyk, M. (2006) Autophagy is involved in T cell death after binding of HIV-1 envelope proteins to CXCR4. *J. Clin. Invest.* **116,** 2161–2172

17. Ullman, E., Fan, Y., Stawowczyk, M., Chen, H. M., Yue, Z., and Zong, W. (2008) Autophagy promotes necrosis in apoptosis-deficient cells in response to ER stress. *Cell Death Differ.* **15,** 422–425
18. Edgell, C. J., McDonald, C. C., and Graham, J. B. (1983) Permanent cell line expressing human factor VIII-related antigen established by hybridization. *Proc. Natl. Acad. Sci. U.S.A.* **80,** 3734–3737
19. Esenabhalu, V. E., Schaeffer, G., and Graier, W. F. (2003) Free fatty acid overload attenuates Ca^{2+} signaling and NO production in endothelial cells. *Antioxid. Redox Signal.* **5,** 147–153
20. Høyer-Hansen, M., Bastholm, L., Szyniarowski, P., Campanella, M., Szabadkai, G., and Farkas, T., Bianchi, K., Fehrenbacher, N., Elling, F., Rizzuto, R., Mathiasen, I. S., and Jäättelä, M. (2007) Control of macroautophagy by calcium, calmodulin-dependent kinase kinase-β, and Bcl-2. *Mol. Cell.* **25,** 193–205
21. Gao, P., Bauvy, C., Souquère, S., Tonelli, G., Liu, L., Zhu, Y., Qiao, Z., Bakula, D., Proikas-Cezanne, T., Pierron, G., Codogno, P., Chen, Q., and Mehrpour, M. (2010) The Bcl-2 homology domain 3 mimetic gossypol induces both Beclin 1-dependent and Beclin 1-independent cytoprotective autophagy in cancer cells. *J. Biol. Chem.* **285,** 25570–25581
22. Stegmeier, F., Sowa, M. E., Nalepa, G., Gygi, S. P., Harper, J. W., and Elledge, S. J. (2007) The tumor suppressor CYLD regulates entry into mitosis. *Proc. Natl. Acad. Sci. U.S.A.* **104,** 8869–8874
23. Naghdi, S., Waldeck-Weiermair, M., Fertschai, I., Poteser, M., Graier, W. F., and Malli, R. (2010) Mitochondrial Ca^{2+} uptake and not mitochondrial motility is required for STIM1-Orai1-dependent store-operated Ca^{2+} entry. *J. Cell Sci.* **123,** 2553–2564
24. Shcherbo, D., Souslova, E. A., Goedhart, J., Chepurnykh, T. V., Gaintzeva, A., Shemiakina, I. I., Gadella, T. W., Lukyanov, S., and Chudakov, D. M. (2009) Practical and reliable FRET/FLIM pair of fluorescent proteins. *BMC Biotechnol.* **9,** 24
25. Roh, M. S., Kim, C. W., Park, B. S., Kim, G. C., Jeong, J. H., Kwon, H. C., Suh, D. J., Cho, K. H., Yee, S. B., and Yoo, Y. H. (2004) Mechanism of histone deacetylase inhibitor trichostatin A-induced apoptosis in human osteosarcoma cells. *Apoptosis* **9,** 583–589
26. Ricchi, M., Odoardi, M. R., Carulli, L., Anzivino, C., Ballestri, S., Pinetti, A., Fantoni, L. I., Marra, F., Bertolotti, M., Banni, S., Lonardo, A., Carulli, N., Loria, P. (2009) Differential effect of oleic and palmitic acid on lipid accumulation and apoptosis in cultured hepatocytes. *J. Gastroenterol. Hepatol.* **24,** 830–840
27. Ilangovan, R., Marshall, W. L., Hua, Y., and Zhou, J. (2003) Inhibition of apoptosis by Z-VAD-fmk in SMN-depleted S2 cells. *J. Biol. Chem.* **278,** 30993–30999
28. Vandenabeele, P., Galluzzi, L., Vanden Berghe, T., and Kroemer, G. (2010) Molecular mechanisms of necroptosis. An ordered cellular explosion. *Nat. Rev. Mol. Cell Biol.* **11,** 700–714
29. Cho, Y. S., Challa, S., Moquin, D., Genga, R., Ray, T. D., Guildford, M., and Chan, F. K. (2009) Phosphorylation-driven assembly of the RIP1-RIP3 complex regulates programmed necrosis and virus-induced inflammation. *Cell* **137,** 1112–1123
30. O'Donnell, M. A., Perez-Jimenez, E., Oberst, A., Ng, A., Massoumi, R., Xavier, R., Green, D. R., and Ting, A. T. (2011) Caspase 8 inhibits programmed necrosis by processing CYLD. *Nat. Cell Biol.* **13,** 1437–1442
31. Kabeya, Y., Mizushima, N., Ueno, T., Yamamoto, A., Kirisako, T., Noda, T., Kominami, E., Ohsumi, Y., and Yoshimori, T. (2000) LC3, a mammalian homologue of yeast Apg8p, is localized in autophagosome membranes after processing. *EMBO J.* **19,** 5720–5728
32. Klionsky, D. J., Abeliovich, H., Agostinis, P., Agrawal, D. K., Aliev, G., Askew, D. S., *et al.* (2008) Guidelines for the use and interpretation of assays for monitoring autophagy in higher eukaryotes. *Autophagy* **4,** 151–175
33. Blommaart, E. F., Krause, U., Schellens, J. P., Vreeling-Sindelárová, H., and Meijer, A. J. (1997) The phosphatidylinositol 3-kinase inhibitors wortmannin and LY294002 inhibit autophagy in isolated rat hepatocytes. *Eur. J. Biochem.* **243,** 240–246
34. Seglen, P. O., and Gordon, P. B. (1982) 3-Methyladenine. Specific inhibitor of autophagic/lysosomal protein degradation in isolated rat hepatocytes. *Proc. Natl. Acad. Sci. U.S.A.* **79,** 1889–1892
35. Grotemeier, A., Alers, S., Pfisterer, S. G., Paasch, F., Daubrawa, M., Dieterle, A., Viollet, B., Wesselborg, S., Proikas-Cezanne, T., and Stork, B. (2010) AMPK-independent induction of autophagy by cytosolic Ca^{2+} increase. *Cell Signal.* **22,** 914–925
36. Tait, S. W., and Green, D. R. (2008) Caspase-independent cell death. Leaving the set without the final cut. *Oncogene* **27,** 6452–6461
37. Tsujimoto, Y. (1997) Apoptosis and necrosis. Intracellular ATP level as a determinant for cell death modes. *Cell Death Differ.* **4,** 429–434
38. Johnson, V. L., Ko, S. C., Holmstrom, T. H., Eriksson, J. E., and Chow, S. C. (2000) Effector caspases are dispensable for the early nuclear morphological changes during chemical-induced apoptosis. *J. Cell Sci.* **113,** 2941–2953
39. Vanlangenakker, N., Bertrand, M. J., Bogaert, P., Vandenabeele, P., and Vanden Berghe, T. (2011) TNF-induced necroptosis in L929 cells is tightly regulated by multiple TNFR1 complex I and II members. *Cell Death Dis.* **2,** e230
40. Upton, J. W., Kaiser, W. J., and Mocarski, E. S. (2010) Virus inhibition of RIP3-dependent necrosis. *Cell Host Microbe.* **7,** 302–313
41. Mei, S., Ni, H. M., Manley, S., Bockus, A., Kassel, K. M., Luyendyk, J. P., Copple, B. L., and Ding, W. X. (2011) Differential roles of unsaturated and saturated fatty acids on autophagy and apoptosis in hepatocytes. *J. Pharmacol. Exp. Ther.* **339,** 487–498
42. Las, G., Serada, S. B., Wikstrom, J. D., Twig, G., and Shirihai, O. S. (2011) Fatty acids suppress autophagic turnover in beta cells. *J. Biol. Chem.* **286,** 42534–42544
43. Csordas, A., Kreutmayer, S., Ploner, C., Braun, P. R., Karlas, A., Backovic, A., Wick, G., and Bernhard, D. (2011) Cigarette smoke extract induces prolonged endoplasmic reticulum stress and autophagic cell death in human umbilical vein endothelial cells. *Cardiovasc. Res.* **92,** 141–148
44. Kroemer, G., and Jäättelä, M. (2005) Lysosomes and autophagy in cell death control. *Nat. Rev. Cancer* **5,** 886–897
45. Gwiazda, K. S., Yang, T. L., Lin, Y., and Johnson, J. D. (2009) Effects of palmitate on ER and cytosolic Ca^{2+} homeostasis in beta cells. *Am. J. Physiol. Endocrinol. Metab.* **296,** E690-E701
46. Zhivotovsky, B., and Orrenius, S. (2011) Calcium and cell death mechanisms. A perspective from the cell death community. *Cell Calcium* **50,** 211–221
47. Fu, M., Li, L., Albrecht, T., Johnson, J. D., Kojic, L. D., and Nabi, I. R. (2011) Autocrine motility factor/phosphoglucose isomerase regulates ER stress and cell death through control of ER calcium release. *Cell Death Differ.* **18,** 1057–1070